Inferring the anthropogenic NO$_x$ emission trend over the United States during 2003 - 2017 from satellite observations: Was there a flattening of the emission trend after the Great Recession?

Jianfeng Li[1], Yuhang Wang[1*]

[1] School of Earth and Atmospheric Sciences, Georgia Institute of Technology, Atlanta, Georgia, USA

[*] *Correspondence to* Yuhang Wang (yuhang.wang@eas.gatech.edu)

Abstract

We illustrate the nonlinear relationships among anthropogenic NO_x emissions, NO_2 tropospheric vertical column densities (TVCDs), and NO_2 surface concentrations using model simulations for July 2011 over the contiguous United States (CONUS). The variations of NO_2 surface concentrations and TVCDs are generally consistent and reflect well anthropogenic NO_x emission variations for high-anthropogenic-NO_x emission regions. For low-anthropogenic-NO_x emission regions, however, nonlinearity in the emission-TVCD relationship due to emissions from lightning and soils, chemistry, and physical processes makes it difficult to use satellite observations to infer anthropogenic NO_x emission changes. The analysis is extended to 2003 – 2017. Similar variations of NO_2 surface measurements and coincident satellite NO_2 TVCDs over urban regions are in sharp contrast to the large variation differences between surface and satellite observations over rural regions. We find a continuous decrease of anthropogenic NO_x emissions after 2011 by examining surface and satellite measurements in CONUS urban regions, but the decreasing rate is lower by 9% - 46% than the pre-2011 period.

1. Introduction

Anthropogenic emissions of nitrogen oxides ($NO_x = NO_2 + NO$) adversely affect the environment, not only because of their direct detrimental impacts on human health (Greenberg et al., 2016; Greenberg et al., 2017; Heinrich et al., 2013; Weinmayr et al., 2009), but also their fundamental roles in the formation of ozone, acid rain, and fine particles which are unfavorable to human health, ecosystem stabilities, and climate change (Crouse et al., 2015; Kampa and Castanas, 2008; Myhre et al., 2013; Pandey et al., 2005; Singh and Agrawal, 2007). About 48.8 Tg N yr^{-1} of NO_x are emitted globally from both anthropogenic (77%) and natural (23%) sources, such as fossil fuel combustion, biomass and biofuel burning, soil bacteria, and lightning (Seinfeld and Pandis, 2016). 3.85 Tg N and 0.24 Tg N of anthropogenic and soil NO_x, respectively, were emitted from the U.S. in 2014 on the basis of the 2014 National Emission Inventory (NEI2014); vehicle sources and fuel combustions accounted for 93% of the total anthropogenic NO_x emissions (EPA, 2017).

The U.S. anthropogenic NO_x emissions during the 2010s declined dramatically compared to the mid-2000s (EPA, 2018; Xing et al., 2013) due to stricter air quality regulations and emission control technology improvements, such as the phase-in of Tier II vehicles during 2004 – 2009 and the switch of power plants from coal to natural gas (De Gouw et al., 2014; McDonald et al., 2018). The overall reduction (about 30% - 50%) of anthropogenic NO_x emissions from the mid-2000s to the 2010s was corroborated by observed decreasing of vehicle NO_x emission factors, NO_2 surface concentrations, nitrate wet deposition flux (Figure S1), and NO_2 tropospheric vertical column densities (TVCDs) (Bishop and Stedman, 2015; Georgoulias et al., 2019; Li et al., 2018; McDonald et al., 2018; Miyazaki et al., 2017; Russell et al., 2012; Tong et al., 2015). However, the detailed NO_x emission changes after the Great Recession (from December 2007 to June 2009) are highly uncertain. On the one hand, the U.S. Environmental Protection Agency

50 (EPA) estimated that the Great Recession had a slight impact on the anthropogenic NO_x emission

51 trend, and the anthropogenic NO_x emissions decreased steadily from 2002 to 2017 (Figure S2),

52 although the emission decrease rate slowed down by about 20% after 2010 (-5.8% yr^{-1} for 2002 –

53 2010, and -4.7% yr^{-1} for 2010 – 2017, Table 1) (EPA, 2018). Fuel-based emission estimates in

54 Los Angeles also showed a steady decrease of anthropogenic NO_x emissions after 2000 and a

55 small impact of the Great Recession on anthropogenic NO_x emission decrease trend (Hassler et

56 al., 2016). The continuous decrease of anthropogenic NO_x emissions was consistent with the

57 ongoing reduction of vehicle emissions (McDonald et al., 2018). On the other hand, Miyazaki et

58 al. (2017) and Jiang et al. (2018) found that the U.S. NO_x emissions derived from satellite NO_2

59 TVCDs, including OMI (the Ozone Monitoring Instrument), SCIAMACHY (SCanning Imaging

60 Absorption SpectroMeter for Atmospheric CHartography), and GOME-2A (Global Ozone

61 Monitoring Experiment – 2 onboard METOP-A), were almost flat from 2010 - 2015 and

62 suggested that the decrease of NO_x emissions was only significant before 2010, which was

63 completely different from the bottom-up and fuel-based emission estimates.

64   A complicating factor in inferring anthropogenic NO_x emission trends from the observations

65 of NO_2 surface concentrations and satellite NO_2 TVCDs is the nonlinearity in NO_x chemistry (Gu

66 et al., 2013; Gu et al., 2016; Lamsal et al., 2011). Although the decrease rates of both NO_2 surface

67 concentrations and coincident OMI NO_2 TVCDs slowed down after the Great Recession over the

68 United States, Tong et al. (2015), Lamsal et al. (2015) and Jiang et al. (2018) found that the

69 slowdown of the decrease rates derived from NO_2 surface concentrations is 12% - 79% less than

70 those of NO_2 TVCDs (Table 1). Secondly, the slowdown of the decrease rates of NO_2 surface

71 concentrations and OMI TVCDs over cities and power plants (Russell et al., 2012; Tong et al.,

72 2015) is significantly less than those over the whole contiguous United States (CONUS) (Jiang et

73 al., 2018; Lamsal et al., 2015). Moreover, Zhang et al. (2018) found that filtering out lightning-

74   affected measurements could significantly improve the comparison of NO$_2$ surface concentration

75   and OMI NO$_2$ TVCD trends over the CONUS.

76   In this study, we carefully investigate the relationships among anthropogenic NO$_x$ emissions,

77   NO$_2$ surface concentrations, and NO$_2$ TVCDs over the CONUS and evaluate the impact of the

78   relationships on inferring anthropogenic NO$_x$ emission changes and trends from surface and

79   satellite observations. Section 2 describes the model and datasets used in this study, including the

80   Regional chEmistry and trAnsport Model (REAM), the EPA Air Quality System (AQS) NO$_2$

81   surface observations, and NO$_2$ TVCD products from OMI, GOME-2A, GOME-2B (GOME2

82   onboard METOP-B), and SCIAMACHY. In Section 3, we examine the nonlinear relationships

83   among anthropogenic NO$_x$ emissions, NO$_2$ surface concentrations, and NO$_2$ TVCDs using model

84   simulations. Accounting for the effects of chemical nonlinearity, we then investigate the

85   anthropogenic NO$_x$ emission trends and changes from 2003 – 2017 over the CONUS. Finally,

86   section 4 gives a summary of the study.

87   2. Model and Data Description

88   2.1 REAM

89   The REAM model has been applied and evaluated in many research applications including

90   ozone simulation and forecast, emission inversion and evaluations, and mechanistic studies of

91   chemical and physical processes (Alkuwari et al., 2013; Cheng et al., 2017; Cheng et al., 2018;

92   Choi et al., 2008a; Choi et al., 2008b; Gu et al., 2013; Gu et al., 2014; Koo et al., 2012; Liu et al.,

93   2012; Liu et al., 2014; Wang et al., 2007; Yang et al., 2011; Zhang et al., 2017; Zhang et al.,

94   2018; Zhang and Wang, 2016; Zhao and Wang, 2009; Zhao et al., 2009a; Zhao et al., 2010).

95   REAM used in this work, the model domain of which is shown in Figure 3, has 30 vertical layers

96   in the troposphere, and the horizontal resolution is 36×36 km^2. The model is driven by

97   meteorology fields from a Weather and Research Forecasting (WRF, version 3.6) model

98   simulation initialized and constrained by the NCEP coupled forecast system model version 2

99   (CFSv2) products (Saha et al., 2011). The chemistry mechanism is based on GEOS-Chem v11.01

100   with updated reaction rates and aerosol uptake of isoprene nitrates (Fisher et al., 2016). Chemistry

101   boundary conditions and initializations are from a GEOS-Chem ($2° \times 2.5°$) simulation. Hourly

102   anthropogenic emissions on weekdays are based on the 2011 National Emission Inventory

103   (NEI2011), while weekend anthropogenic emissions are set to be two-thirds of the weekday

104   emissions (Beirle et al., 2003; Choi et al., 2012). Biogenic VOC emissions are estimated using the

105   Model of Emissions of Gases and Aerosols from Nature (MEGAN) v2.10 (Guenther et al., 2012).

106   NO_x emissions from soils are based on the Yienger and Levy (YL) scheme (Li et al., 2019;

107   Yienger and Levy, 1995). The cloud-to-ground (CG) lightning flashes are calculated following

108   Choi et al. (2005) and Zhao et al. (2009a) with the parameterization of CG flash rate as a function

109   of convective mass fluxes and convective available potential energy (CAPE). The ratios of intra-

110   cloud (IC) lightning flashes to CG flashes are parameterized as a function of the height between

111   the freezing layer and the cloud top (Luo et al., 2017; Price and Rind, 1992). In this study, 250

112   moles of NO are emitted per CG or IC flash (Zhao et al., 2009a). As a result, on weekdays in July

113   2011, REAM has mean anthropogenic NO_x emissions of 7.4×10^{10} molecules $cm^{-2} s^{-1}$, mean soil

114   NO_x emissions of 1.2×10^{10} molecules $cm^{-2} s^{-1}$, and mean lightning NO_x emissions of 3.4×10^{10}

115   molecules $cm^{-2} s^{-1}$ over the CONUS.

116   **2.2 Satellite NO_2 TVCDs**

117   In this study, we use NO_2 TVCD products from four satellite sensors in the past decade,

118   including SCIAMACHY, GOME-2A, GOME-2B, and OMI, the spectrometers onboard sun-

119   synchronous satellites to monitor atmospheric trace gases. The SCIAMACHY instrument

120   onboard the Environmental Satellite (ENVISAT) has an equator overpass time of 10:00 Local

121   time (LT) and a nadir pixel resolution of 60×30 km^2. The GOME-2 instruments on Metop-A

122   (named as GOME-2A) and Metop-B (GOME-2B) satellites cross the equator at 9:30 LT and have

123   a nadir resolution of 80×40 km^2. After July 15, 2013, the nadir resolution of GOME-2A became

124   40×40 km^2 with a smaller scanning swath. The OMI onboard the EOS-Aura satellite has a nadir

125   resolution of 24×13 km^2 and overpasses the equator around 13:45 LT. More detailed

126   information about these instruments is summarized in Table S1. These instruments measure

127   backscattered solar radiation from the atmosphere in the ultraviolet and visible wavelength. The

128   radiation measurements in the wavelength of 402 - 465 nm are then used to retrieve NO_2 VCDs.

129   The retrieval process consists of three steps: 1) converting radiation observations to NO_2 slant

130   column densities (SCDs) by using the Differential Optical Absorption Spectroscopy (DOAS)

131   spectral fitting method; 2) separating tropospheric SCDs and stratospheric SCDs from the total

132   NO_2 SCDs; 3) dividing the NO_2 tropospheric SCDs by the tropospheric air mass factors (AMF) to

133   compute VCDs.

134   The product archives we use in this study include GOME-2B (TM4NO2A v2.3),

135   SCIAMACHY (QA4ECV v1.1), GOME-2A (QA4ECV v1.1), OMI (QA4ECV v1.1, hereafter

136   referred to as OMI-QA4ECV), OMNO2 (SPv3, hereafter referred to as OMI-NASA), and the

137   Berkeley High-Resolution NO_2 products (v3.0B, hereafter referred to as OMI-BEHR). OMI-

138   BEHR uses the tropospheric SCDs from OMI-NASA products but updates some inputs for the

139   tropospheric AMF calculation (Laughner et al., 2018). These product archives have been

140   previously validated (Boersma et al., 2018; Drosoglou et al., 2017; Drosoglou et al., 2018;

141   Krotkov et al., 2017; Laughner et al., 2018; Wang et al., 2017; Zara et al., 2018). Generally, the

142   pixel-size uncertainties of these products are > 30% over polluted regions under clear-sky

143   conditions. We summarize the basic information about these products in Table S2. To keep the

144   high quality and sampling consistency of NO_2 TVCD datasets, we chose pixel-size NO_2 TVCD

145   data using the criteria listed in Table S3. After the selection, we re-gridded the pixel-size data into

146   the REAM 36×36 km^2 grid cells and calculate the seasonal means of each grid cell with

147   corresponding daily values on weekdays (winter: January, February, and December; spring:

148   March, April, and May; summer: June, July, and Autumn; autumn: September, October, and

149   November). We excluded weekend data in this study to minimize the impacts of weekend NO_x

150   emission reduction, leading to different NO_2 TVCDs between weekdays and weekends (Figure

151   S3).

152   Satellite TVCD measurements can show large variations and apparent discontinuities due in

153   part to the effects of cloud, lightning NO_x, the shift of satellite pixel coverage, and retrieval

154   uncertainties (Figure S3; e.g., (Boersma et al., 2018; Zhang et al., 2018)). However, continuous

155   and consistent measurements are required for reliable trend analyses. In addition to the criteria of

156   data selection in Table S3, we compute the seasonal relative 90th percentile confidence interval,

157   defined as RCI = (X(95th percentile) - X(5th percentile)) / mean(X), where X is the daily NO_2

158   TVCD for a given season. To compute the seasonal trend, we require that RCI is < 50% for the

159   selected season every year in the analysis period (Table S3). About 45% of data are removed as a

160   result.

161   **2.3 Surface NO_2 measurements**

162   Hourly surface NO_2 measurements from 2003 - 2017 are from the EPA AQS monitoring

163   network (archived on https://www.epa.gov/outdoor-air-quality-data). Most AQS monitoring sites

164   use the Federal Reference Method (FRM) — gas-phase chemiluminescence to measure NO_2. Few

165   sites use the Federal Equivalent Method (FEM) – photolytic-chemiluminescence or the Cavity

166   Attenuated Phase Shift Spectroscopy (CAPS) method. FRM and FEM are indirect methods, in

167   which NO_2 is first converted to NO and then NO is measured through chemiluminescence

168   measurement of NO_2^* produced by $NO + O_3$. The difference is that FRM uses heated

169   reducers/catalysts for the conversion of NO_2 to NO and FEM uses photolysis of NO_2 to NO. The

170   conversion to NO in the FRM instruments is not specific to NO_2, and non-NO_x active nitrogen

171 compounds (NO_z) can also be reduced by the catalysts, which would cause high biases of NO_2

172 measurements, while the FEM method is sensitive to the photolysis conversion efficiency of NO_2

173 to NO (Beaver et al., 2012; Beaver et al., 2013; Lamsal et al., 2015). The CAPS method directly

174 determines NO_2 concentrations based on a NO_2-induced phase shift measured by a photodetector.

175 The CAPS instrument operates at a wavelength of about 450 nm and may overestimate NO_2

176 concentrations due to absorption of other molecules at the same wavelength (Beaver et al., 2012;

177 Beaver et al., 2013; Kebabian et al., 2005).

178   Due to the different characteristics of the above three methods and demonstrated biases

179 between the FRM and the FEM by Lamsal et al. (2015), we firstly investigate the measurement

180 discrepancies among the above three methods. There are three sites having FRM and FEM

181 measurements simultaneously during some periods from 2013 - 2014, two sites having both FRM

182 and CAPS data during some periods from 2015 – 2016, and one site using all three measurement

183 methods during some periods in 2015. Figure S4 shows the hourly averaged ratios of FEM and

184 CAPS to FRM data, respectively, for 4 seasons during 2013 – 2016. The CAPS/FRM ratios are in

185 the range of 0.94 – 1.06 and the FEM/FRM ratios of 0.86 – 1.11. Furthermore, Zhang et al.

186 (2018) discussed that the relative trends are not affected by scaling the observation data. As in the

187 work by Zhang et al. (2018), we analyze the relative trends in the surface NO_2 data. We,

188 therefore, did not scale the FRM data. At sites with FEM or CAPS measurements, we use these

189 measurements in place of FRM data. If both FEM and CAPS data are available, we use the

190 averages of the two datasets.

191   Since NO_2 surface concentrations have significant diurnal variations (Figure S5), we choose

192 the data at 9:00-10:00 LT for comparison with GOME-2A/2B data, 10:00-11:00 LT for

193 comparison with SCIAMACHY data, and 13:00-14:00 LT for OMI data. The seasonal *RCI* <

194 50% requirement is also used here to be consistent with the analysis of satellite TVCD data, and

195 thus about 1.5% of the data are removed. We also require that the measurement site must have

196   valid measurements in the aforementioned 3 hours for at least one season from 2003 – 2017. The

197   locations of the 179 selected sites using the site selection criteria are shown in Figure 1. The

198   region definitions follow the U.S. Census Bureau (https://www2.census.gov/geo/pdfs/maps-

199   data/maps/reference/us_regdiv.pdf).

3. Results and Discussions

3.1 Nonlinear relationships among anthropogenic NO_x emissions, NO_2 surface concentrations, and NO_2 TVCDs

203   NO_2 surface concentrations and NO_2 TVCD are not linearly correlated with NO_x emissions

204   due in part to chemical nonlinearity, wet and dry depositions, transport effects, background

205   sources (Gu et al., 2013; Lamsal et al., 2011). Therefore, it is necessary to first investigate the

206   nonlinearities among NO_x emissions, NO_2 surface concentrations, and TVCDs over the CONUS

207   before we compare the trends between NO_2 surface concentrations and TVCDs. The nonlinearity

208   between NO_x emission and NO_2 TVCD is analyzed by examining the local sensitivity of NO_2

209   TVCD to NO_x emissions (Gu et al., 2013; Lamsal et al., 2011; Tong et al., 2015), which is

210   defined as β in Equation (1). We further define γ as the sensitivity of NO_2 surface concentration

211   to NO_x emission:

$$\frac{\Delta E}{E} = \beta \frac{\Delta \Omega}{\Omega} \tag{1}$$

$$\frac{\Delta E}{E} = \gamma \frac{\Delta c}{c} \tag{2}$$

214   where E denotes NO_x emission and ΔE denotes the change of NO_x emission; Ω denotes NO_2

215   TVCD, c denotes surface NO_2 concentration, and $\Delta \Omega$ and Δc denote the corresponding changes.

216   We computed β and γ values for July 2011 over the CONUS using REAM. To compute

217   local β and γ values, we added another independent group of chemistry species ("group 2") in

218   REAM in order to compute the standard and sensitivity simulations concurrently. The original

219   chemical species in the model ("group 1") were used in the standard simulation. For group 2

220   chemical species, anthropogenic NO_x emissions were reduced by 15%. In the model simulation,

221   we first computed the advection of group 1 tracers. The horizontal tracer fluxes were therefore

222   available. All influxes into a grid cell for group 2 tracer simulation were from group 1 tracer

223   simulation; only outfluxes were computed using group 2 tracers. The outflux was one way in that

224   nitrogen species were transported out but the transport did not affect adjacent grid cells because

225   the influxes were from group 1 tracer simulation. Using this procedure, the effects of

226   anthropogenic NO_x emission reduction were localized. The β and γ values were computed by the

227   ratio of TVCD and surface concentration changes to 15% change of anthropogenic NO_x

228   emissions, respectively.

229   Figure 2 shows the distributions of our β and γ ratios as a function of anthropogenic NO_x

230   emissions for July 2011 over the CONUS. Results essentially the same as Figure 2 were obtained

231   when a perturbation of 10% was used for anthropogenic NO_x emissions. Figure S6 shows the

232   distributions of NO_2 TVCD fraction in the boundary layer at 13:00 – 14:00 LT and 10:00 – 11:00

233   LT, and the fraction of soil NO_x emissions in all surface sources (soil + anthropogenic) on

234   weekdays for July 2011, respectively. In Figure S7, we analyzed the contributions of background

235   sources and non-emission factors (transport, chemistry, and wet and dry depositions) to the

236   nonlinear relationships (β and γ) among anthropogenic NO_x emissions, NO_2 surface

237   concentrations, and NO_2 TVCDs. While the model simulation is for one summer month, several

238   key points on the surface and column concentration sensitivities to anthropogenic NO_x emissions

239   have implications for comparing the trends of AQS and satellite TVCD data. (1) Both β and γ

240   values are negatively correlated with anthropogenic NO_x emissions due to chemical nonlinearity,

241   transport, and background NO_x contributions (Figures 2, S6, and S7) (Gu et al., 2016; Lamsal et

242   al., 2011). It is consistent with the distribution of β as a function of NO_x emissions in China (Gu

243   et al., 2013), although the β ratios for the US are generally larger than for China due primarily to

244   different emission distributions of NO_x and VOCs and regional circulation patterns (Zhao et al.,

245   2009b). (2) The uncertainties of β and γ values increase significantly as anthropogenic NO_x

246   emissions decrease, which means regions with low anthropogenic NO_x emissions are more

247   sensitive to environmental conditions, such as NO_x transport from nearby regions which may

248   even produce negative β and γ values (Figures 2 and S7). (3) The value of γ is generally less than

249   β, especially for low-anthropogenic-NO_x emission regions, which reflects the significant

250   contribution of free tropospheric NO_2 to NO_2 TVCD but not to NO_2 surface concentrations

251   (Figures 2, S6, and S7). (4) The variations of β and γ values in anthropogenic NO_x emission bins

252   tend to be larger at 10:00 – 11:00 than at 13:00 – 14:00 LT, reflecting a stronger transport effect

253   due to weaker chemical losses at 10:00 – 11:00 (Figure 2). (5) Both β and γ values are

254   significantly less than 1 at 13:00 – 14:00 LT ($\beta = 0.74$ and $\gamma = 0.84$) when anthropogenic NO_x

255   emissions are $> 4 \times 10^{12}$ molecules cm^{-2} s^{-1}, but they are close to 1 at 10:00 – 11:00 LT ($\beta = 0.96$

256   and $\gamma = 1.02$), which reflect stronger chemistry nonlinearity at 13:00 – 14:00 than in the morning

257   (Figure 2). (6) Both background sources and non-emission factors contribute much more to β and

258   γ values in low-anthropogenic-NO_x emission regions than in high-anthropogenic-NO_x emission

259   regions (Figure S7). (7) Generally, non-emission factors contribute more to β and γ values than

260   background sources in low-anthropogenic-NO_x emission regions (Figures S7c and S7d) except

261   for the first bin where background sources contribute more to β and γ values than non-emission

262   factors at 10:00 – 11:00, which is partly caused by some grid cells with extremely low

263   anthropogenic NO_x emissions, increasing the mean contributions of background sources in the

264   first bin.

265   The largely varying β and γ values for anthropogenic NO_x emissions $< 10^{11}$ molecules cm^{-2}

266   s^{-1} imply that the trends derived from satellite TVCD data do not directly represent anthropogenic

267   NO_x emissions and that the variations of TVCD data may not be comparable to the corresponding

268   surface NO_2 concentrations. We define a region "urban" if anthropogenic NO_x emissions from

269   NEI2011 are $> 10^{11}$ molecules cm^{-2} s^{-1}. All the other regions are defined as "rural". Figure 3

270   shows the distributions of anthropogenic NO_x emissions and urban and rural regions defined in

271   this study. Such defined urban regions account for 69.8% of the total anthropogenic NO_x

272   emissions over the CONUS, the trend of which is, therefore, representative of anthropogenic

273   emission changes. A caveat is that some "urban" regions would become "rural" if anthropogenic

274   NO_x emissions decreased after 2011 as the EPA anthropogenic NO_x emission trend suggested

275   (Figure S2). In a sensitivity study, we define an urban region using a stricter criterion of

276   anthropogenic NO_x emissions $> 2 \times 10^{11}$ molecules cm^{-2} s^{-1} and the analysis results are similar to

277   those shown in the next section.

278   **3.2 Trend comparisons between NO_2 AQS surface concentrations and coincident**

279   **satellite NO_2 tropospheric VCD over urban and rural regions**

280   By using anthropogenic NO_x emissions of 10^{11} molecules cm^{-2} s^{-1} as the threshold value, 157

281   AQS sites are urban, and the rest 22 sites are rural. Their properties are summarized in Table 2.

282   Figure 4 shows the relative annual variations of AQS NO_2 surface measurements at 13:00 – 14:00

283   and coincident OMI-QA4ECV NO_2 TVCD data from 2005 – 2017 in each season for urban and

284   rural regions. The contrast between the two regions is apparent in all seasons. For comparison

285   purposes, we scale the time series of TVCD and AQS surface NO_2 to their corresponding 2005

286   values, and the resulting data are therefore unitless. Over urban regions, NO_2 surface

287   concentrations are highly correlated with NO_2 TVCDs (TVCD $= 1.03 \times$ AQS $+ 0.11$, $R^2 = 0.98$),

288   reflecting the comparable and stable β and γ values (Figure 2). However, over rural regions, the

289   scaled TVCD data significantly deviate from AQS NO_2 data (TVCD $= 1.15 \times$ AQS $+ 0.09$, $R^2 =$

290   0.87). It is noteworthy that the discrepancies between urban and rural data are smaller in winter

291   than in spring, summer, and autumn due to a more dominant role of transport than chemistry and

292   lower natural NO_x emissions in winter.

293   We also examine the correlations of AQS NO_2 surface concentrations with coincident OMI-

294   NASA, OMI-BEHR, SCIAMACHY, GOME-2A, and GOME-2B TVCD measurements. The

295   results of OMI-NASA and OMI-BEHR are similar to those of OMI-QA4ECV (Figure 4).

296   SCIAMACHY and GOME-2B TVCD observations at 9:00-11:00 LT also show large contrast

297   between urban (SCIAMACHY: TVCD = $0.92 \times$ AQS - 0.005, R^2 = 0.94; GOME-2B: TVCD =

298   $0.54 \times$ AQS + 0.56, R^2 = 0.96) and rural regions (SCIAMACHY: TVCD = $0.77 \times$ AQS +0.83, R^2

299   = 0.63; GOME-2B: TVCD = $0.46 \times$ AQS + 0.73, R^2 = 0.59). The correlation of coincident

300   GOME-2A NO_2 TVCD data with AQS surface concentrations is poor for rural (TVCD = $0.65 \times$

301   AQS + 0.56, R^2 = 0.44) and urban (TVCD = $0.31 \times$ AQS + 0.56, R^2 = 0.21) regions (Figure S8),

302   which likely reflects the degradation of the GOME-2A instrument causing significant increase of

303   NO_2 SCD uncertainties (Boersma et al., 2018). Therefore, we excluded GOME-2A in the analysis

304   hereafter.

305   We further investigate OMI-QA4ECV NO_2 TVCD relative annual variations from 2005 -

306   2017 over the regions with different anthropogenic NO_x emissions in Figure 5. We find clear

307   flattening of NO_2 TVCD variations as anthropogenic NO_x emissions decrease, which is consistent

308   with the above analysis. Similar to Figure 4, the spread of TVCD variation is much less in winter

309   than the other seasons. The differences between Figures 5 and 4 are due to a much larger dataset

310   used in the former than the latter. Only coincident AQS and OMI-QA4ECV data are used in

311   Figure 4, but all OMI-KMNI data are used in Figure 5.

3.3 Trend analysis of AQS NO₂ surface concentrations, satellite TVCDs, and updated EPA NOx emissions

We first updated the CEMS measurement data used in the EPA NO_x emission trend datasets with the newest datasets obtained from https://ampd.epa.gov/ampd/. As shown in Figure S2, the updated CEMS data lead to a reduction of anthropogenic NO_x emissions during the Great Recession (2008 – 2009) and a recovery period in 2010 – 2011. The sharp drop during the Great Recession and the flattening trend right after the Great Recession are captured by OMI NO_2 and SCIAMACHY TVCD products (Figures 4, 6, and S9) and AQS NO_2 surface measurements (Figures 4, 6, and S5) and are also noted by Russell et al. (2012) and Tong et al. (2015) (Table 1).

In Figure 6, we show the comparisons among the relative variations of the updated EPA anthropogenic NO_x emissions, AQS NO_2 surface measurements at 10:00-11:00 and 13:00-14:00, and coincident satellite NO_2 TVCDs for urban regions in 4 seasons from 2003 to 2017. Also shown are the comparisons among the updated EPA anthropogenic NO_x emissions and satellite NO_2 TVCDs. There are many more data points for the latter comparison because the data selection is no longer limited to those coincident with the AQS surface data, and therefore, the uncertainty spread is much lower. The comparisons, in general, show consistent results that the updated EPA anthropogenic NO_x emissions, AQS surface measurements, and satellite TVCD data are in agreement. The agreement of decreasing trends among the datasets is just as good for the post-2011 period as the pre-2011 period. This result differs from Miyazaki et al. (2017) and Jiang et al. (2018), who suggested no significant decreasing trend for OMI TVCD data and inversed NO_x emissions after 2010. The disagreement can be explained by the results of Figure 5. Including the low anthropogenic NO_x emission regions leads to underestimates of NO_x decreases. Since the area of low anthropogenic NO_x emission regions is larger than high anthropogenic NO_x emission regions (Table 2), the arithmetic averaging will lead to a large weighting of rural observations, which do not reflect anthropogenic NO_x emission changes. Miyazaki et al. (2017)

337 and Jiang et al. (2018) included all regions in their analyses, but we exclude rural regions. Figure

338 S9 shows the seasonal variations if the TVCDs over rural regions are included; the result shows a

339 much lower decreasing rate of TVCDs over the CONUS. The much slower satellite TVCD trends

340 for regions with low NO_x emissions was previously discussed by Zhang et al. (2018). In addition,

341 Miyazaki et al. (2017) and Jiang et al. (2018) conducted NO_x emission inversions by using the

342 Model for Interdisciplinary Research on Climate (MIROC)-Chem with a coarse resolution of 2.8°

343 × 2.8°, which was insufficient to separate urban and rural regions and might distort predicted NO_2

344 TVCDs and inversed NO_x emissions due to nonlinear effects (Valin et al., 2011; Yu et al., 2016),

345 which is another possible reason for their find of flattening NO_x emission trends after 2010.

346   We summarize the decreasing rates of NO_2 after the Great Recession in Table 3. To

347 minimize the effect of the sharp decrease and the subsequent recovery, we chose to analyze the

348 post-2011 period. Table 3 summarizes the results for each season, while Table 1 gives the

349 averaged annual decreasing trends. Generally, Tables 1 and 3 confirm the continuous decreases of

350 AQS surface observations, satellite NO_2 TVCD, and updated EPA anthropogenic NO_x emissions

351 after 2011 as in Figure 6, but the decreasing rates are lower than the pre-2011 period. Over the

352 AQS urban sites, the slowdown magnitudes are 9% for AQS surface observations and 20% - 40%

353 for satellite NO_2 TVCD measurements, which may reflect in part smaller γ than β values (Table

354 2). Our estimated slowdown magnitudes are significantly lower than Lamsal et al. (2015) and

355 Jiang et al. (2018) (Table 1), which might be caused by their different data processing methods,

356 such as including AQS sites with incomplete measurement records (Silvern et al., 2019).

357   Over the CONUS urban regions, updated EPA anthropogenic NO_x emissions show a

358 slowdown of 22% compared to 29% - 46% for three OMI NO_2 TVCD products. The difference is

359 partially due to the β ratio of 2.5 ± 1.0 at 13:00 – 14:00 over the CONUS urban regions (Table 2).

360 Satellite NO_2 TVCD measurement uncertainties also contribute to the difference. From 2013 –

361 2017, GOME-2B NO_2 TVCDs decrease more than OMI products, especially in spring, autumn

362 and winter (Tables 1 and 3). Finally, trend analyses in different regions (Figure 7 and Table S4)

363 indicate that generally, the Midwest has the least slowdown of the decreasing rate for urban OMI

364 NO_2 TVCD (-14% on average) after 2011 compared to the Northeast (-30%), South (-34%), and

365 West (-28%).

366   The results presented in this study are qualitatively in agreement with the work by Silvern et

367 al. (2019). The two studies were independent. Therefore, the foci of the studies are different

368 despite reaching similar conclusions. While we focused on understanding the detailed data

369 analysis of Jiang et al. (2018) and limited the use of model simulation results so that our results

370 can be compared to the previous study directly, Silvern et al. (2019) relied more on multi-year

371 model simulations. As a result, Silvern et al. (2019) can clearly identify the contributions of the

372 NO_2 columns by natural emissions and make use of additional observations such as nitrate

373 deposition fluxes. They also identified model biases in simulating the trends of NO_2 TVCDs by

374 missing natural emissions in the free troposphere. Our study, on the other hand, explored the data

375 analysis procedure through which the trend of anthropogenic emissions can be derived from

376 satellite observations and its limitations.

377 4. Conclusions

378   Using model simulations for July 2017, we demonstrate the nonlinear relationship of NO_2

379 surface concentration and TVCD with anthropogenic NO_x emissions. Over low anthropogenic

380 NO_x emission regions, the ratios of anthropogenic NO_x emission changes to the changes of

381 surface concentrations (γ) and TVCDs (β) have very large variations and $\beta > \gamma \gg 1$.

382 Therefore, for the same emission changes, surface concentration and TVCD changes are much

383 smaller and variable than urban regions, making it difficult to use the observations to directly

384 infer anthropogenic NO_x emission trends. We find that defining urban regions where

385 anthropogenic NO_x emissions are $> 10^{11}$ molecules cm^{-2} s^{-1} and using surface and TVCD

386   observations over these regions can infer the trends that can be compared with the EPA emission

387   trend estimates.

388   We evaluate the anthropogenic NO_x emission variations from 2003 – 2017 over the CONUS

389   by using satellite NO_2 TVCD products from GOME-2B, SCIAMACHY, OMI-QA4ECV, OMI-

390   NASA, and OMI-BEHR, over the urban regions of CONUS. We find broad agreements among

391   the decreases of AQS NO_2 surface observations, satellite NO_2 TVCD products, and the EPA

392   anthropogenic NO_x emissions with the CEMS dataset updated. After 2011, they all show a

393   slowdown of the decreasing rates. Over the AQS urban sites, NO_2 surface concentrations have a

394   slowdown of 9% and OMI products show a slowdown of 20% - 40%. Over the CONUS urban

395   regions, OMI TVCD products indicate a slowdown of 29% - 46%, and the updated EPA

396   anthropogenic NO_x emissions have a slowdown of 22%. The different slowdown magnitudes

397   between OMI TVCD products and the other two datasets may be caused by the nonlinear

398   response of TVCD to anthropogenic emissions and the uncertainties of satellite measurements

399   (e.g., GOME-2B TVCD data show a larger decreasing trend than OMI products from 2013 –

400   2017).

401   We did not find observation evidence supporting the notion that anthropogenic NO_x

402   emissions have not been decreasing after the Great Recession. In future studies, we recommend

403   that the nonlinear relationships of NO_x emissions with NO_2 TVCD and surface concentration be

404   carefully evaluated when applying satellite and surface measurements to infer the changes of

405   anthropogenic NO_x emissions.

406   **Data availability**

407   The EPA AQS hourly surface NO_2 measurements are downloaded from

408   https://aqs.epa.gov/aqsweb/airdata/download_files.html#Raw. QA4ECV 1.1 NO_2 VCD products

409   (OMI-QA4ECV, GOME-2A, and SCIAMACHY) are from http://temis.nl/qa4ecv/no2col/data/.

410   GOME-2B NO_2 VCD products are from

411   http://www.temis.nl/airpollution/no2col/no2colgome2b.php. OMI-BEHR and OMI-NASA

412   archives are from http://behr.cchem.berkeley.edu/DownloadBEHRData.aspx. REAM simulation

413   results for this study are available upon request.

414   **Author contribution**

415   JL and YW designed the study. JL conducted model simulations and data analyses with

416   discussions with YW. JL and YW wrote the manuscript.

417   **Competing interests**

418   The authors declare that they have no conflict of interest.

419   **Acknowledgments**

420   This work was supported by the NASA ACMAP Program. We thank Ruixiong Zhang for

421   discussions with J. Li. Thank Benjamin Wells, Alison Eyth, Lee Tooly from EPA, the EPA

422   MOVES team, Betty Carter from COORDINATING RESEARCH COUNCIL, INC., Brain

423   McDonald from NOAA, and Zhe Jiang from University of Science and Technology of China for

424   helping us an understanding of the NEI MOVES mobile source emissions.

References

426   Alkuwari, F. A., Guillas, S., and Wang, Y.: Statistical downscaling of an air quality model using
427   Fitted Empirical Orthogonal Functions, Atmos. Environ., 81, 1-10,
428   10.1016/j.atmosenv.2013.08.031, 2013.

429   Beaver, M., Long, R., and Kronmiller, K.: Characterization and Development of Measurement
430   Methods for Ambient Nitrogen Dioxide (NO_2), National Air Quality Conference - Ambient Air
431   Monitoring 2012, Denver, CO, US, 2012.

Beaver, M., Kronmiller, K., Duvall, R., Kaushik, S., Morphy, T., King, P., and Long, R.: Direct and Indirect Methods for the Measurement of Ambient Nitrogen Dioxide, AWMA Measurement Technologies meeting, Sacramento, CA, US, 2013.

Beirle, S., Platt, U., Wenig, M., and Wagner, T.: Weekly cycle of NO_2 by GOME measurements: A signature of anthropogenic sources, Atmos. Chem. Phys., 3, 2225-2232, 10.5194/acp-3-2225-2003, 2003.

Bishop, G. A., and Stedman, D. H.: Reactive nitrogen species emission trends in three light-/medium-duty United States fleets, Environ. Sci. Technol., 49, 11234-11240, 10.1021/acs.est.5b02392, 2015.

Boersma, K. F., Eskes, H. J., Richter, A., De Smedt, I., Lorente, A., Beirle, S., van Geffen, J. H., Zara, M., Peters, E., and Roozendael, M. V.: Improving algorithms and uncertainty estimates for satellite NO_2 retrievals: results from the quality assurance for the essential climate variables (QA4ECV) project, Atmos. Meas. Tech., 11, 6651-6678, 10.5194/amt-11-6651-2018, 2018.

Cheng, Y., Wang, Y., Zhang, Y., Chen, G., Crawford, J. H., Kleb, M. M., Diskin, G. S., and Weinheimer, A. J.: Large biogenic contribution to boundary layer O_3-CO regression slope in summer, Geophys. Res. Lett., 44, 7061-7068, 10.1002/2017GL074405, 2017.

Cheng, Y., Wang, Y., Zhang, Y., Crawford, J. H., Diskin, G. S., Weinheimer, A. J., and Fried, A.: Estimator of surface ozone using formaldehyde and carbon monoxide concentrations over the eastern United States in summer, J. Geophys. Res.-Atmos., 123, 7642-7655, 10.1029/2018JD028452, 2018.

Choi, Y., Wang, Y., Zeng, T., Martin, R. V., Kurosu, T. P., and Chance, K.: Evidence of lightning NO_x and convective transport of pollutants in satellite observations over North America, Geophys. Res. Lett., 32, 10.1029/2004GL021436, 2005.

Choi, Y., Wang, Y., Yang, Q., Cunnold, D., Zeng, T., Shim, C., Luo, M., Eldering, A., Bucsela, E., and Gleason, J.: Spring to summer northward migration of high O_3 over the western North Atlantic, Geophys. Res. Lett., 35, 10.1029/2007GL032276, 2008a.

Choi, Y., Wang, Y., Zeng, T., Cunnold, D., Yang, E. S., Martin, R., Chance, K., Thouret, V., and Edgerton, E.: Springtime transitions of NO_2, CO, and O_3 over North America: Model evaluation and analysis, J. Geophys. Res.-Atmos., 113, 10.1029/2007JD009632, 2008b.

Choi, Y., Kim, H., Tong, D., and Lee, P.: Summertime weekly cycles of observed and modeled NO_x and O_3 concentrations as a function of satellite-derived ozone production sensitivity and land use types over the Continental United States, Atmos. Chem. Phys., 12, 6291-6307, 10.5194/acp-12-6291-2012, 2012.

Crouse, D. L., Peters, P. A., Hystad, P., Brook, J. R., van Donkelaar, A., Martin, R. V., Villeneuve, P. J., Jerrett, M., Goldberg, M. S., and Pope III, C. A.: Ambient $PM_{2.5}$, O_3, and NO_2 exposures and associations with mortality over 16 years of follow-up in the Canadian Census Health and Environment Cohort (CanCHEC), Environ. Health Perspect., 123, 1180, 10.1289/ehp.1409276, 2015.

470 De Gouw, J. A., Parrish, D. D., Frost, G. J., and Trainer, M.: Reduced emissions of CO2, NO_x,
471 and SO_2 from US power plants owing to switch from coal to natural gas with combined cycle
472 technology, Earth's Future, 2, 75-82, 10.1002/2013EF000196, 2014.

473 Drosoglou, T., Bais, A. F., Zyrichidou, I., Kouremeti, N., Poupkou, A., Liora, N., Giannaros, C.,
474 Koukouli, M. E., Balis, D., and Melas, D.: Comparisons of ground-based tropospheric NO_2
475 MAX-DOAS measurements to satellite observations with the aid of an air quality model over the
476 Thessaloniki area, Greece, Atmos. Chem. Phys., 17, 5829-5849, 10.5194/acp-17-5829-2017,
477 2017.

478 Drosoglou, T., Koukouli, M. E., Kouremeti, N., Bais, A. F., Zyrichidou, I., Balis, D., Xu, J., and
479 Li, A.: MAX-DOAS NO_2 observations over Guangzhou, China; ground-based and satellite
480 comparisons, Atmos. Meas. Tech., 11, 2239-2255, 10.5194/amt-11-2239-2018, 2018.

481 EPA: PROFILE OF VERSION 1 OF THE 2014 NATIONAL EMISSIONS INVENTORY, U.S.
482 Environmental Protection Agency, 2017.

483 Air Pollutant Emissions Trends Data: https://www.epa.gov/air-emissions-inventories/air-
484 pollutant-emissions-trends-data, 2018.

485 Fisher, J. A., Jacob, D. J., Travis, K. R., Kim, P. S., Marais, E. A., Chan Miller, C., Yu, K., Zhu,
486 L., Yantosca, R. M., and Sulprizio, M. P.: Organic nitrate chemistry and its implications for
487 nitrogen budgets in an isoprene-and monoterpene-rich atmosphere: constraints from aircraft
488 ($SEAC^4RS$) and ground-based (SOAS) observations in the Southeast US, Atmos. Chem. Phys.,
489 16, 5969-5991, 10.5194/acp-16-5969-2016, 2016.

490 Georgoulias, A. K., van der A, R. J., Stammes, P., Boersma, K. F., and Eskes, H. J.: Trends and
491 trend reversal detection in 2 decades of tropospheric NO_2 satellite observations, Atmos. Chem.
492 Phys., 19, 6269-6294, 10.5194/acp-19-6269-2019, 2019.

493 Greenberg, N., Carel, R. S., Derazne, E., Bibi, H., Shpriz, M., Tzur, D., and Portnov, B. A.:
494 Different effects of long-term exposures to SO_2 and NO_2 air pollutants on asthma severity in
495 young adults, J. Toxicol. Environ. Health, A, 79, 342-351, 10.1080/15287394.2016.1153548,
496 2016.

497 Greenberg, N., Carel, R. S., Derazne, E., Tiktinsky, A., Tzur, D., and Portnov, B. A.: Modeling
498 long-term effects attributed to nitrogen dioxide (NO_2) and sulfur dioxide (SO_2) exposure on
499 asthma morbidity in a nationwide cohort in Israel, J. Toxicol. Environ. Health, A, 80, 326-337,
500 10.1080/15287394.2017.1313800, 2017.

501 Gu, D., Wang, Y., Smeltzer, C., and Liu, Z.: Reduction in NO_x emission trends over China:
502 Regional and seasonal variations, Environ. Sci. Technol., 47, 12912-12919, 10.1021/es401727e,
503 2013.

504 Gu, D., Wang, Y., Smeltzer, C., and Boersma, K. F.: Anthropogenic emissions of NO_x over
505 China: Reconciling the difference of inverse modeling results using GOME-2 and OMI
506 measurements, J. Geophys. Res.-Atmos., 119, 7732-7740, 10.1002/2014JD021644, 2014.

507 Gu, D., Wang, Y., Yin, R., Zhang, Y., and Smeltzer, C.: Inverse modelling of NO_x emissions over
508 eastern China: uncertainties due to chemical non-linearity, Atmos. Meas. Tech., 9, 5193-5201,
509 10.5194/amt-9-5193-2016, 2016.

510 Guenther, A. B., Jiang, X., Heald, C. L., Sakulyanontvittaya, T., Duhl, T., Emmons, L. K., and
511 Wang, X.: The Model of Emissions of Gases and Aerosols from Nature version 2.1
512 (MEGAN2.1): an extended and updated framework for modeling biogenic emissions, Geosci.
513 Model Dev., 5, 1471-1492, 10.5194/gmd-5-1471-2012, 2012.

514 Hassler, B., McDonald, B. C., Frost, G. J., Borbon, A., Carslaw, D. C., Civerolo, K., Granier, C.,
515 Monks, P. S., Monks, S., and Parrish, D. D.: Analysis of long-term observations of NO_x and CO
516 in megacities and application to constraining emissions inventories, Geophys. Res. Lett., 43,
517 9920-9930, 10.1002/2016GL069894, 2016.

518 Heinrich, J., Thiering, E., Rzehak, P., Krämer, U., Hochadel, M., Rauchfuss, K. M., Gehring, U.,
519 and Wichmann, H.-E.: Long-term exposure to NO_2 and PM_{10} and all-cause and cause-specific
520 mortality in a prospective cohort of women, Occup. Environ. Med., 70, 179-186, 10.1136/oemed-
521 2012-100876, 2013.

522 Jiang, Z., McDonald, B. C., Worden, H., Worden, J. R., Miyazaki, K., Qu, Z., Henze, D. K.,
523 Jones, D. B. A., Arellano, A. F., and Fischer, E. V.: Unexpected slowdown of US pollutant
524 emission reduction in the past decade, Proc. Natl. Acad. Sci. U.S.A., 201801191,
525 10.1073/pnas.1801191115, 2018.

526 Kampa, M., and Castanas, E.: Human health effects of air pollution, Environ. Pollut., 151, 362-
527 367, 10.1016/j.envpol.2007.06.012, 2008.

528 Kebabian, P. L., Herndon, S. C., and Freedman, A.: Detection of nitrogen dioxide by cavity
529 attenuated phase shift spectroscopy, Anal. Chem., 77, 724-728, 10.1021/ac048715y, 2005.

530 Koo, J.-H., Wang, Y., Kurosu, T. P., Chance, K., Rozanov, A., Richter, A., Oltmans, S. J.,
531 Thompson, A. M., Hair, J. W., and Fenn, M. A.: Characteristics of tropospheric ozone depletion
532 events in the Arctic spring: analysis of the ARCTAS, ARCPAC, and ARCIONS measurements
533 and satellite BrO observations, Atmos. Chem. Phys., 12, 9909-9922, 10.5194/acp-12-9909-2012,
534 2012.

535 Krotkov, N. A., Lamsal, L. N., Celarier, E. A., Swartz, W. H., Marchenko, S. V., Bucsela, E. J.,
536 Chan, K. L., Wenig, M., and Zara, M.: The version 3 OMI NO_2 standard product, Atmos. Meas.
537 Tech., 10, 3133-3149, 10.5194/amt-10-3133-2017, 2017.

538 Lamsal, L. N., Martin, R. V., Padmanabhan, A., Van Donkelaar, A., Zhang, Q., Sioris, C. E.,
539 Chance, K., Kurosu, T. P., and Newchurch, M. J.: Application of satellite observations for timely
540 updates to global anthropogenic NO_x emission inventories, Geophys. Res. Lett., 38,
541 10.1029/2010GL046476, 2011.

542 Lamsal, L. N., Duncan, B. N., Yoshida, Y., Krotkov, N. A., Pickering, K. E., Streets, D. G., and
543 Lu, Z.: US NO_2 trends (2005–2013): EPA Air Quality System (AQS) data versus improved
544 observations from the Ozone Monitoring Instrument (OMI), Atmos. Environ., 110, 130-143,
545 10.1016/j.atmosenv.2015.03.055, 2015.

546 Laughner, J. L., Zhu, Q., and Cohen, R. C.: The Berkeley High Resolution Tropospheric NO_2
547 product, Earth System Science Data, 10, 2069-2095, 10.5194/essd-10-2069-2018, 2018.

548 Li, J., Mao, J., Fiore, A. M., Cohen, R. C., Crounse, J. D., Teng, A. P., Wennberg, P. O., Lee, B.
549 H., Lopez-Hilfiker, F. D., and Thornton, J. A.: Decadal changes in summertime reactive oxidized
550 nitrogen and surface ozone over the Southeast United States, Atmos. Chem. Phys., 18, 2341-
551 2361, 10.5194/acp-18-2341-2018, 2018.

552 Li, J., Wang, Y., and Qu, H.: Dependence of summertime surface ozone on NO_x and VOC
553 emissions over the United States: Peak time and value, Geophys. Res. Lett., 46, 3540-3550,
554 10.1029/2018GL081823, 2019.

555 Liu, Z., Wang, Y., Vrekoussis, M., Richter, A., Wittrock, F., Burrows, J. P., Shao, M., Chang, C.
556 C., Liu, S. C., and Wang, H.: Exploring the missing source of glyoxal (CHOCHO) over China,
557 Geophys. Res. Lett., 39, 10.1029/2012GL051645, 2012.

558 Liu, Z., Wang, Y., Costabile, F., Amoroso, A., Zhao, C., Huey, L. G., Stickel, R., Liao, J., and
559 Zhu, T.: Evidence of aerosols as a media for rapid daytime HONO production over China,
560 Environ. Sci. Technol., 48, 14386-14391, 10.1021/es504163z, 2014.

561 Luo, C., Wang, Y., and Koshak, W. J.: Development of a self-consistent lightning NO_x
562 simulation in large-scale 3-D models, J. Geophys. Res.-Atmos., 122, 3141-3154,
563 10.1002/2016JD026225, 2017.

564 McDonald, B., McKeen, S., Cui, Y. Y., Ahmadov, R., Kim, S.-W., Frost, G. J., Pollack, I.,
565 Peischl, J., Ryerson, T. B., and Holloway, J.: Modeling Ozone in the Eastern US using a Fuel-
566 Based Mobile Source Emissions Inventory, Environ. Sci. Technol., 10.1021/acs.est.8b00778,
567 2018.

568 Miyazaki, K., Eskes, H., Sudo, K., Boersma, K. F., Bowman, K., and Kanaya, Y.: Decadal
569 changes in global surface NO_x emissions from multi-constituent satellite data assimilation,
570 Atmos. Chem. Phys, 17, 807-837, 10.5194/acp-17-807-2017, 2017.

571 Myhre, G., Shindell, D., Bréon, F.-M., Collins, W., Fuglestvedt, J., Huang, J., Koch, D.,
572 Lamarque, J.-F., Lee, D., Mendoza, B., Nakajima, T., Robock, A., Stephens, G., Takemura, T.,
573 and Zhang, H.: Anthropogenic and natural radiative forcing, in: Climate change 2013: The
574 Physical Science Basis. Contribution of Working Group I to the Fifth Assessment Report of the
575 Intergovernmental Panel on Climate Change, Cambridge University Press, Cambridge, United
576 Kingdom and New York, NY, USA, 659-740, 2013.

577 Pandey, J. S., Kumar, R., and Devotta, S.: Health risks of NO_2, SPM and SO_2 in Delhi (India),
578 Atmos. Environ., 39, 6868-6874, 10.1016/j.atmosenv.2005.08.004, 2005.

579 Price, C., and Rind, D.: A simple lightning parameterization for calculating global lightning
580 distributions, J. Geophys. Res.-Atmos., 97, 9919-9933, 10.1029/92JD00719, 1992.

581 Russell, A. R., Valin, L. C., and Cohen, R. C.: Trends in OMI NO_2 observations over the United
582 States: effects of emission control technology and the economic recession, Atmos. Chem. Phys.,
583 12, 12197-12209, 10.5194/acp-12-12197-2012, 2012.

584 Seinfeld, J. H., and Pandis, S. N.: Atmospheric chemistry and physics: from air pollution to
585 climate change, John Wiley & Sons, Inc, Hoboken, New Jersey, 2016.

586 Silvern, R. F., Jacob, D. J., Mickley, L. J., Sulprizio, M. P., Travis, K. R., Marais, E. A., Cohen,
587 R. C., Laughner, J. L., Choi, S., Joiner, J., and Lamsal, L. N.: Using satellite observations of
588 tropospheric NO_2 columns to infer long-term trends in US NO_x emissions: the importance of
589 accounting for the free tropospheric NO_2 background, Atmos. Chem. Phys., 19, 8863-8878,
590 10.5194/acp-19-8863-2019, 2019.

591 Singh, A., and Agrawal, M.: Acid rain and its ecological consequences, J. Environ. Biol., 29, 15,
592 2007.

593 Tong, D., Lamsal, L., Pan, L., Ding, C., Kim, H., Lee, P., Chai, T., Pickering, K. E., and Stajner,
594 I.: Long-term NO_x trends over large cities in the United States during the great recession:
595 Comparison of satellite retrievals, ground observations, and emission inventories, Atmos.
596 Environ., 107, 70-84, 10.1016/j.atmosenv.2015.01.035, 2015.

597 Valin, L. C., Russell, A. R., Hudman, R. C., and Cohen, R. C.: Effects of model resolution on the
598 interpretation of satellite NO_2 observations, Atmos. Chem. Phys., 11, 11647-11655, 10.5194/acp-
599 11-11647-2011, 2011.

600 Wang, Y., Choi, Y., Zeng, T., Davis, D., Buhr, M., Huey, L. G., and Neff, W.: Assessing the
601 photochemical impact of snow NO_x emissions over Antarctica during ANTCI 2003, Atmos.
602 Environ., 41, 3944-3958, 10.1016/j.atmosenv.2007.01.056, 2007.

603 Wang, Y., Beirle, S., Lampel, J., Koukouli, M., De Smedt, I., Theys, N., Ang, L., Wu, D., Xie, P.,
604 and Liu, C.: Validation of OMI, GOME-2A and GOME-2B tropospheric NO_2, SO_2 and HCHO
605 products using MAX-DOAS observations from 2011 to 2014 in Wuxi, China: investigation of the
606 effects of priori profiles and aerosols on the satellite products, Atmos. Chem. Phys., 17, 5007,
607 10.5194/acp-17-5007-2017, 2017.

608 Weinmayr, G., Romeo, E., De Sario, M., Weiland, S. K., and Forastiere, F.: Short-term effects of
609 PM_{10} and NO_2 on respiratory health among children with asthma or asthma-like symptoms: a
610 systematic review and meta-analysis, Environ. Health Perspect., 118, 449-457,
611 10.1289/ehp.0900844, 2009.

612 Xing, J., Pleim, J., Mathur, R., Pouliot, G., Hogrefe, C., Gan, C. M., and Wei, C.: Historical
613 gaseous and primary aerosol emissions in the United States from 1990 to 2010, Atmos. Chem.
614 Phys., 13, 7531-7549, 10.5194/acp-13-7531-2013, 2013.

615 Yang, Q., Wang, Y., Zhao, C., Liu, Z., Gustafson Jr, W. I., and Shao, M.: NO_x emission reduction
616 and its effects on ozone during the 2008 Olympic Games, Environ. Sci. Technol., 45, 6404-6410,
617 10.1021/es200675v, 2011.

618 Yienger, J. J., and Levy, H.: Empirical model of global soil-biogenic NO_x emissions, J. Geophys.
619 Res.-Atmos., 100, 11447-11464, 10.1029/95JD00370, 1995.

620 Yu, K., Jacob, D. J., Fisher, J. A., Kim, P. S., Marais, E. A., Miller, C. C., Travis, K. R., Zhu, L.,
621 Yantosca, R. M., and Sulprizio, M. P.: Sensitivity to grid resolution in the ability of a chemical

622 transport model to simulate observed oxidant chemistry under high-isoprene conditions, Atmos.
623 Chem. Phys., 16, 4369-4378, 10.5194/acp-16-4369-2016, 2016.

624 Zara, M., Boersma, K. F., De Smedt, I., Richter, A., Peters, E., Van Geffen, J. H. G. M., Beirle,
625 S., Wagner, T., Van Roozendael, M., and Marchenko, S.: Improved slant column density retrieval
626 of nitrogen dioxide and formaldehyde for OMI and GOME-2A from QA4ECV: intercomparison,
627 uncertainty characterization, and trends, Meas. Tech. Discuss, 1-47, 10.5194/amt-11-4033-2018,
628 2018.

629 Zhang, R., Wang, Y., He, Q., Chen, L., Zhang, Y., Qu, H., Smeltzer, C., Li, J., Alvarado, L., and
630 Vrekoussis, M.: Enhanced trans-Himalaya pollution transport to the Tibetan Plateau by cut-off
631 low systems, Atmos. Chem. Phys., 17, 3083-3095, 10.5194/acp-17-3083-2017, 2017.

632 Zhang, R., Wang, Y., Smeltzer, C., Qu, H., Koshak, W., and Boersma, K. F.: Comparing OMI-
633 based and EPA AQS in situ NO_2 trends: towards understanding surface NO_x emission changes,
634 Atmos. Meas. Tech., 11, 3955-3967, 10.5194/amt-11-3955-2018, 2018.

635 Zhang, Y., and Wang, Y.: Climate-driven ground-level ozone extreme in the fall over the
636 Southeast United States, Proc. Natl. Acad. Sci. U.S.A., 113, 10025-10030,
637 10.1073/pnas.1602563113, 2016.

638 Zhao, C., and Wang, Y.: Assimilated inversion of NO_x emissions over east Asia using OMI NO_2
639 column measurements, Geophys. Res. Lett., 36, 10.1029/2008GL037123, 2009.

640 Zhao, C., Wang, Y., Choi, Y., and Zeng, T.: Summertime impact of convective transport and
641 lightning NO_x production over North America: modeling dependence on meteorological
642 simulations, Atmos. Chem. Phys., 9, 4315-4327, 10.5194/acp-9-4315-2009, 2009a.

643 Zhao, C., Wang, Y., and Zeng, T.: East China plains: A "basin" of ozone pollution, Environ. Sci.
644 Technol., 43, 1911-1915, 10.1021/es8027764, 2009b.

645 Zhao, C., Wang, Y., Yang, Q., Fu, R., Cunnold, D., and Choi, Y.: Impact of East Asian summer
646 monsoon on the air quality over China: View from space, J. Geophys. Res.-Atmos., 115,
647 10.1029/2009JD012745, 2010.

648

Table 1. Summary of trends of satellite NO_2 TVCD products, NO_2 surface measurements, and EPA anthropogenic NO_x emissions during from different studies

Studies	Datasets	Period 1[1]		Period 2		Period 3		Slowdown ratio[3]
		Time	Trend (yr⁻¹)[2]	Time	Trend (yr⁻¹)	Time	Trend (yr⁻¹)	
This study for CONUS "urban" sites[4]	GOME-2B[5] (36×36 km^2)					2013 - 2017	**-8.2 ± 3.0%**	
	SCIAMACHY (36×36 km^2)	2003 – 2011	**-6.3 ± 1.1%**					
	OMI-NASA (36×36 km^2)	2005 – 2011	**-8.6 ± 1.2%**			2011 – 2016	**-6.1 ± 3.6%**	**-29%**[2]
	OMI-BEHR (36×36 km^2)	2005 – 2011	**-8.2 ± 1.3%**			2011 – 2016	**-4.4 ± 1.6%**	**-46%**
	OMI-QA4ECV (36×36 km^2)	2005 – 2011	**-7.7 ± 1.4%**			2011 - 2017	**-4.2 ± 0.5%**	**-46%**
	Updated EPA NO_x emissions[6]	2003 – 2011	**-6.5 ± 0.8%**			2011 - 2017	**-5.1 ± 0.3%**	**-22%**
This study for AQS "urban" sites	GOME-2B (36×36 km^2)					2013 - 2017	**-10.2 ± 2.9%**	
	SCIAMACHY (36×36 km^2)	2003 - 2011	**-7.6 ± 1.1%**					
	OMI-NASA (36×36 km^2)	2005 - 2011	**-9.0 ± 0.8%**			2011 – 2016	**-7.2 ± 3.8%**	**-20%**
	OMI-BEHR (36×36 km^2)	2005 - 2011	**-8.9 ± 0.3%**			2011 – 2016	**-6.2 ± 2.6%**	**-30%**
	OMI-QA4ECV (36×36 km^2)	2005 - 2011	**-9.0 ± 0.8%**			2011 - 2017	**-5.4 ± 0.9%**	**-40%**
	NO_2 surface VMR[7]	2003 - 2011	**-6.5 ± 1.2%**			2011 - 2017	**-5.9 ± 0.8%**	**-9%**
(Russell et al., 2012)[8]	BEHR v2.1 NO_2 TVCD ($0.05° \times 0.05°$)	2005 - 2007	-6 ± 5% **(-6.2%)**[9]	2007 - 2009	-8 ± 5% **(-8.4%)**	2009 - 2011	-3 ± 4% **(-3.0%)**	**-52%**
	Updated EPA NO_x emissions		**-6.0%**		**-10.0%**		**-2.4%**	**-60%**
(Tong et al., 2015)[10]	NASA v2.1 NO_2 TVCD (pixels $< 50 \times 24$ km^2)		-7.3% **(-7.6%)**		-9.2% **(-11.4%)**		-2.8% **(-4.4%)**	**-42%**
	BEHR v2.1 NO_2 TVCD (pixels $< 50 \times 24$ km^2)	2005 - 2007	-8.9% **(-9.3%)**	2008 - 2009	-9.1% **(-11.8%)**	2010 - 2012	-3.6% **(-6.0%)**	**-35%**
	NO_2 surface VMR		-6.0% **(-6.2%)**		-10.8% **(-13.2%)**		-3.4% **(-5.4%)**	**-13%**
	Updated EPA NO_x emissions		**-6.0%**		**-10.0%**		**-3.4%**	**-43%**
(Lamsal et al., 2015)[11]	NASA v2.1 NO_2 TVCD ($0.1° \times 0.1°$)		-4.8 ± 1.9% **(-5.1%)**				-1.2 ± 1.2% **(-1.2%)**	**-76%**
	NO_2 surface VMR	2005 - 2008	-3.7 ± 1.5% **(-3.8%)**			2010 - 2013	-2.1 ± 1.4% **(-2.1%)**	**-45%**
	Updated EPA NO_x emissions		**-6.4%**				**-4.0%**	**-38%**
(Jiang et al., 2018)[11]	NASA v3 NO_2 TVCD ($0.5° \times 0.667°$)		-10.2 ± 1.8% **(-9.8%)**				-3.2 ± 1.6% **(-3.2%)**	**-67%**
	QA4ECV v2 NO_2 TVCD ($0.5° \times 0.667°$)		-9.6 ± 1.7% **(-9.3%)**				-2.6 ± 1.8% **(-2.6%)**	**-72%**
	BEHR v2.1 NO_2 TVCD ($0.5° \times 0.667°$)	2005 - 2009	-8.5 ± 1.8% **(-8.2%)**			2011-2015	-2.1 ± 1.6% **(-2.1%)**	**-74%**
	NO_2 surface VMR		-6.6 ± 1.4% **(-6.4%)**				-2.6 ± 1.5% **(-2.6%)**	**-59%**
	Updated EPA NO_x emissions		**-7.8%**				**-5.0%**	**-36%**

650 [1] Since different studies used different time division methods, we list the period of each study in the table.
651 [2] Trends are based on an exponential model ($E(y) = E_0 \times r^{y-y_0}$: "$y$" denotes year and "$y_0$" denotes the initial year; "$E(y)$" denotes the value at year "y" and "E_0" denotes the value at the initial year; r-1 is the relative trend).
652 [3] Slowdown ratios = Trend in "period 3" / Trend in "period 1" – 1.
653 [4] Trends in our study are calculated based on the national seasonal trends shown in Table 3.
654 [5] The information on satellite products used in this study is summarized in Table S2.
655 [6] We updated EPA anthropogenic NO_x emissions with the newest Continuous Emission Monitoring Systems (CEMS) datasets. Figure S2 shows the comparison between our updated and original EPA anthropogenic NO_x emissions (EPA, 2018).
656 [7] Denote the averaged trends of 13:00 and 10:00 LT based on the values in Table 3.

657   [8] The study used NO_2 TVCD from urban and power plant grid cells across the U.S.

658   [9] Since previous studies used linear models to calculate trends and the results are sensitive to their calculation methods and the selection of initial years, we recalculate the trends based on the above exponential model, which makes all the results

659   consistent. Our results are those bold numbers inside the parentheses, while the numbers in normal fonts are from the original publications.

660   [10] The study uses NO_2 TVCD and surface concentrations from Los Angeles, Dallas, Houston, Atlanta, Philadelphia, Washington, D.C., New York, and Boston.

661   [11] The two studies used the EPA Air Quality System (AQS) NO_2 surface measurements and coincident satellite NO_2 TVCD data over the U.S.

662   **Table 2.** Properties of urban and rural regions in July 2011

type	Surface area fraction[1]	Anthropogenic NO_x emissions ($\times 10^{10}$ molecules cm^{-2} s^{-1})	β at 13:00 – 14:00 LT	γ at 13:00 – 14:00 LT	β at 10:00 – 11:00 LT	γ at 10:00 – 11:00 LT
Urban/CONUS[2]	17.3%	29.9	2.5 ± 1.0	1.5 ± 0.4	2.6 ± 1.9	1.6 ± 1.2
Rural/CONUS	82.7%	2.7	16.9 ± 16.4	8.5 ± 11.7	12.2 ± 14.0	6.4 ± 11.6
Urban/AQS	87.7%	71.0	1.6 ± 0.8	1.2 ± 0.4	1.7 ± 1.1	1.3 ± 0.6
Rural/AQS	12.3%	5.7	8.7 ± 9.9	5.2 ± 8.8	5.4 ± 15.1	3.8 ± 11.7

663   [1] "Fraction" denotes the percentages of "urban" or "rural" data points for the whole CONUS or all AQS sites.
664   [2] "Urban-CONUS" denote CONUS "urban" grid cells; "Urban-AQS" denote AQS "urban" site grid cells.
665
666

667 **Table 3.** Summary of national trends of updated EPA anthropogenic NO_x emissions, AQS NO_2 surface concentrations at 13:00 – 14:00 and 10:00 – 11:00 LT, and satellite NO_2 TVCD products for 4 seasons
668 during different periods[1]

		Spring		Summer		Autumn		Winter	
		AQS site	CONUS	AQS site	CONUS	AQS site	CONUS	AQS site	CONUS
AQS NO_2 VMR at 13:00 -14:00	2003 – 2011	-7.3 ± 1.4%		-7.4 ± 0.9%		-6.7 ± 1.8%		-5.2 ± 0.8%	
	2011 – 2017	-5.3 ± 1.6%		-6.4 ± 1.2%		-7.3 ± 2.5%		-6.0 ± 2.8%	
AQS NO_2 VMR at 10:00 – 11:00	2003 – 2011	-7.1 ± 1.6%		-7.6 ± 1.5%		-6.2 ± 2.2%		-4.4 ± 1.6%	
	2011 – 2017	-4.4 ± 1.4%		-6.1 ± 1.8%		-6.3 ± 2.5%		-5.2 ± 2.4%	
SCIAMACHY	2003 – 2011	-8.8 ± 3.4%	-6.9 ± 1.1%	-8.2 ± 1.6%	-5.2 ± 1.2%	-6.8 ± 2.4%	-5.6 ± 2.1%	-6.4 ± 7.4%	-7.5 ± 5.5%
	2011 – 2017								
GOME2B	2003 – 2011								
	2013 – 2017	-10.2 ± 7.8%	-8.3 ± 16.9%	-6.4 ± 14.0%	-5.3 ± 4.0%	-10.5 ± 41.6%	-6.9 ± 13.2%	-13.6 ± 15.1%	-12.3 ± 78.9%
OMI-QA4ECV	2005 – 2011	-9.3 ± 5.6%	-8.3 ± 4.6%	-8.3 ± 2.4%	-5.9 ± 5.2%	-10.0 ± 4.2%	-7.4 ± 2.4%	-8.3 ± 2.1%	-9.3 ± 5.2%
	2011 – 2017	-5.3 ± 6.0%	-4.3 ± 6.5%	-4.2 ± 3.0%	-4.9 ± 9.2%	-6.0 ± 1.8%	-3.8 ± 1.8%	-6.1 ± 25.6%	-3.8 ± 3.5%
OMI-NASA	2005 – 2011	-9.4 ± 5.0%	-9.6 ± 5.3%	-9.4 ± 2.8%	-7.1 ± 2.9%	-9.4 ± 3.2%	-8.1 ± 2.8%	-7.8 ± 3.6%	-9.5 ± 16.6%
	2011 – 2016	-4.4 ± 18.9%	-3.8 ± 7.5%	-5.7 ± 6.7%	-4.5 ± 5.3%	-6.0 ± 3.1%	-4.6 ± 3.9%	-12.8 ± 7.8%	-11.4 ± 6.6%
OMI-BEHR	2005 – 2011	-9.1 ± 5.3%	-8.9 ± 5.8%	-8.7 ± 2.4%	-6.4 ± 3.2%	-9.2 ± 3.2%	-8.0 ± 3.1%	-8.5 ± 10.6%	-9.4 ± 23.0%
	2011 – 2016	-3.8 ± 4.4%	-3.0 ± 4.0%	-5.4 ± 7.0%	-3.9 ± 6.6%	-5.6 ± 13.2%	-4.1 ± 14.0%	-9.9 ± 5.2%	-6.7 ± 5.9%
EPA	2003 – 2011	-6.5 ± 0.8%							
	2011 – 2017	-5.1 ± 0.3%							

669 [1] We calculate trends by using the exponential model described in Table 1.
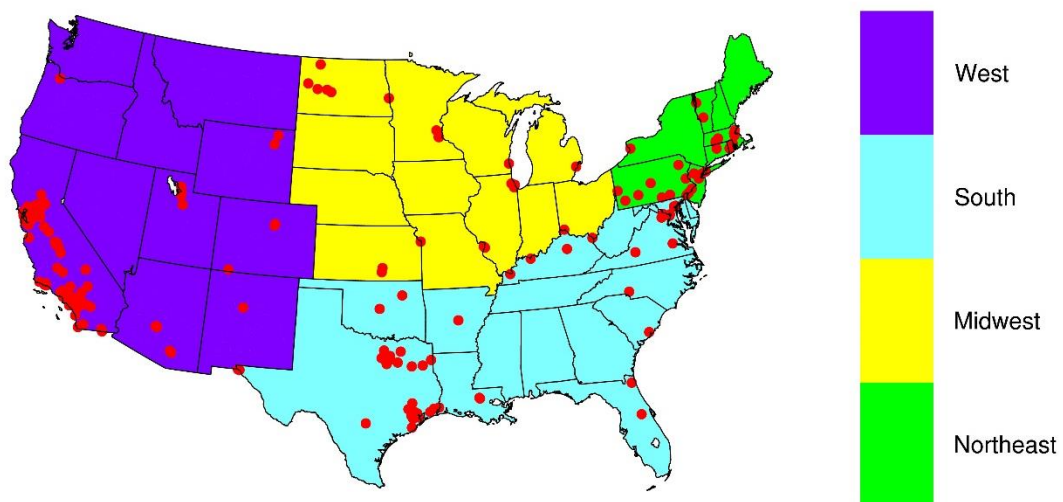
670
671   Figure 1. Region definitions and locations of NO_2 surface observation sites used in this study.

672
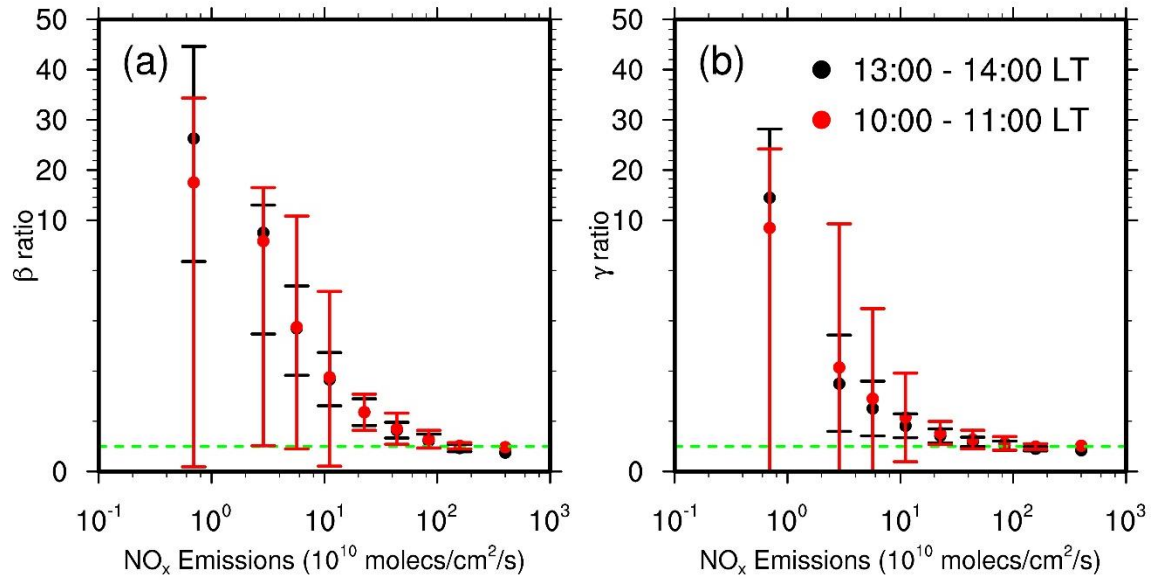
Figure 2. Distributions of β (panel a) and γ (panel b) ratios as a function of anthropogenic NO_x emissions on weekdays for July 2011 over the CONUS. "13:00 – 14:00 LT" is for OMI, and "10:00 – 11:00" LT is for SCIAMACHY and GOME-2A/2B. The data are binned into nine groups based on anthropogenic NO_x emissions: $E \in (0, 2^1), [2^1, 2^2), [2^2, 2^3), [2^3, 2^4), [2^4, 2^5), [2^5, 2^6), [2^6, 2^7), [2^7, 2^8), [2^8, 2^9) \times 10^{10}$ molecules cm^{-2} s^{-1}. Here, $(0, 2^1)$ denotes $0 <$ emissions $< 2^1$, and $[2^1, 2^2)$ denotes $2^1 \leq$ emissions $< 2^2$, similar to other intervals. The green dashed line denotes a value of 1. Error bars denote standard deviations.
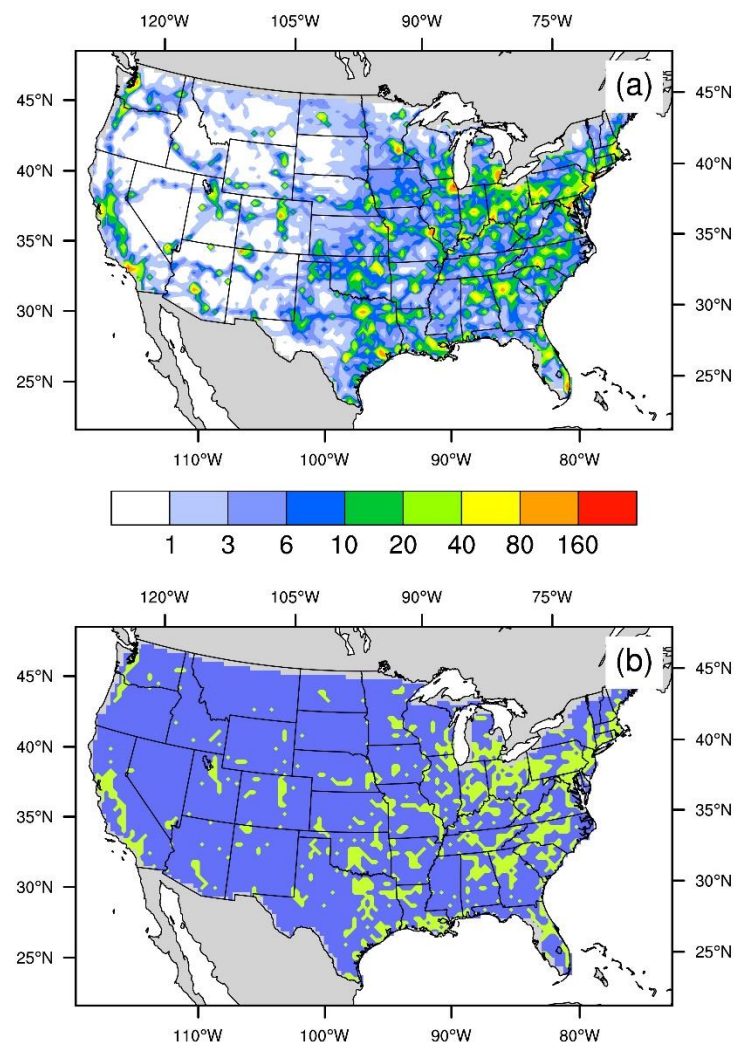
682
683 Figure 3. Spatial distributions of (a) anthropogenic NO_x emissions (unit: 10^{10} molecules cm^{-2} s^{-1})
684 and (b) "urban" regions satisfying our selection criteria. In (b), light green and blue denote the
685 resulting urban and rural regions, respectively.

686
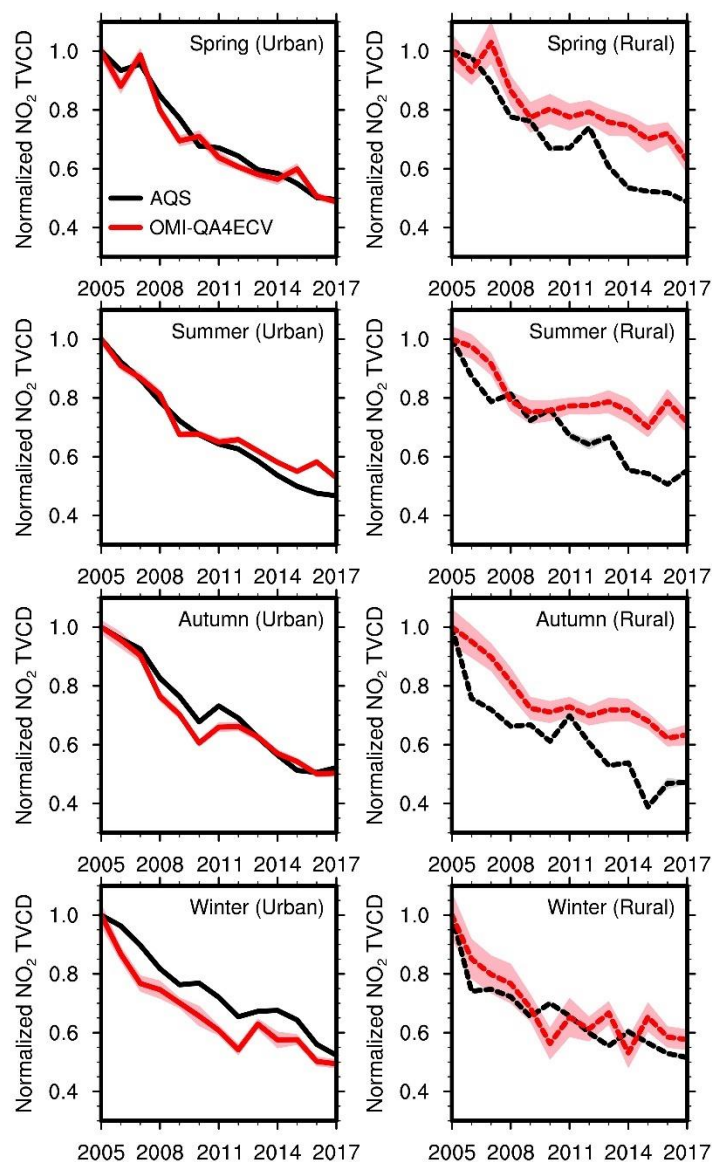
Figure 4. Relative annual variations of AQS NO$_2$ surface concentrations and coincident OMI-QA4ECV NO$_2$ TVCD in each season from 2005 – 2017 for urban (left panel) and rural (right panel) regions. The observation data are scaled by the corresponding 2005 values. Black and red lines denote AQS surface observations and OMI-QA4ECV NO$_2$ TVCDs, respectively. Shading in a lighter color is added to show the standard deviation of the results; when uncertainty is small due in part to a large number of data points, shading area may not show up.
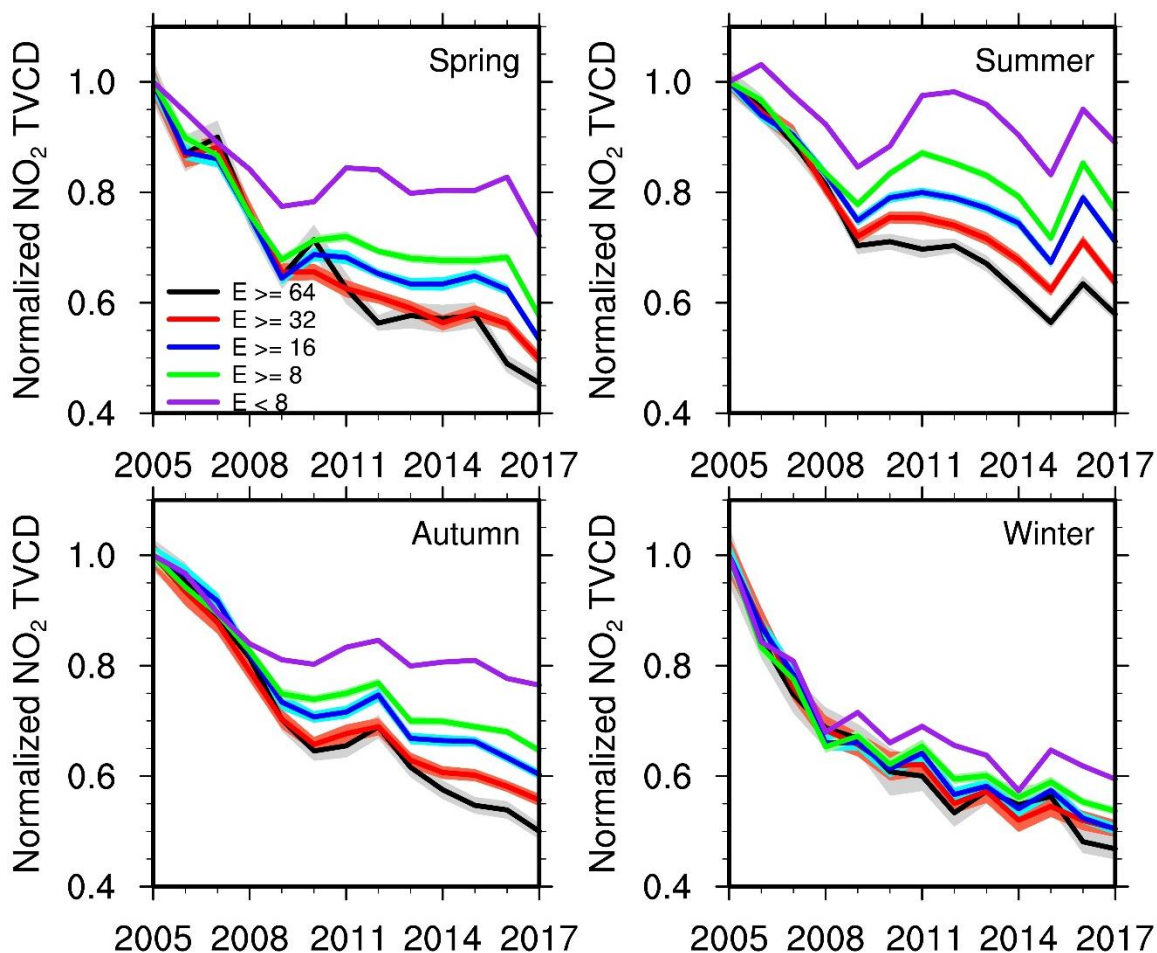
Figure 5. Relative annual variations of OMI-QA4ECV NO_2 TVCD for different anthropogenic NO_x-emission groups based on NEI2011 in each season from 2005 – 2017. "E >= 64" denotes grid cells with anthropogenic NO_x emissions over 64×10^{10} molecules cm^{-2} s^{-1}. "E >= 32" denotes grid cells with anthropogenic NO_x emissions equal to or larger than 32×10^{10} molecules cm^{-2} s^{-1} but less than 64×10^{10} molecules cm^{-2} s^{-1}. "E >= 16" and "E >= 8" have similar meanings as "E >= 32". "E < 8" denotes grid cells with anthropogenic NO_x emissions less than 8×10^{10} molecules cm^{-2} s^{-1}. Shading in a lighter color is added to show the standard deviation of the results; when uncertainty is small due in part to a large number of data points, shading area may not show up.
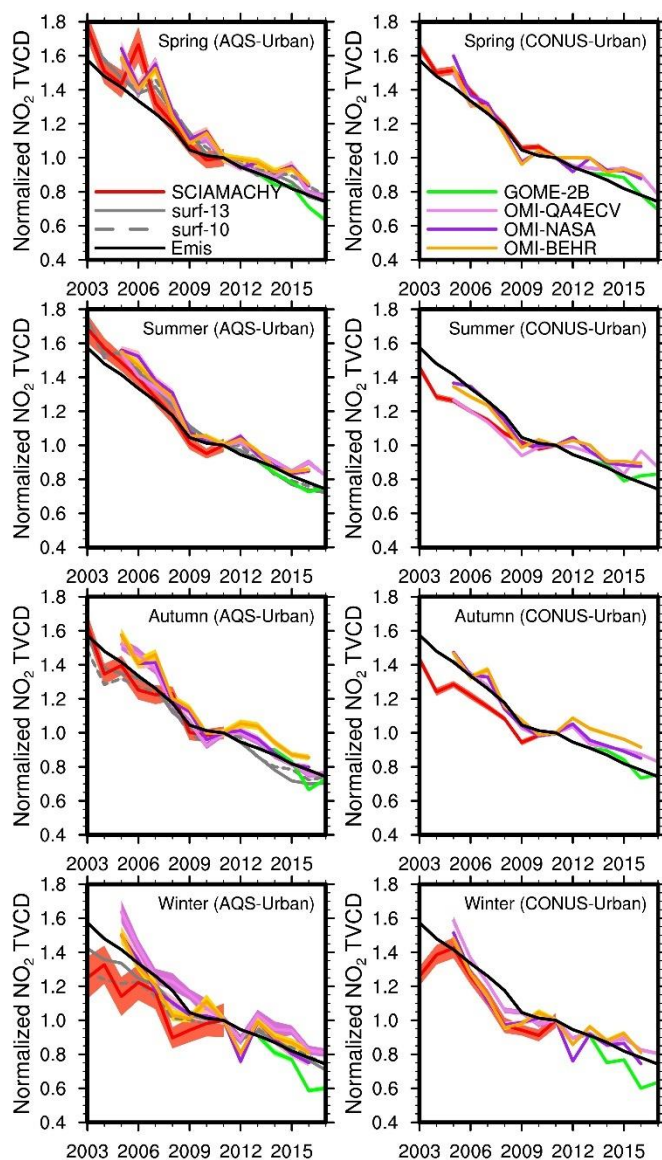
Figure 6. Relative variations of AQS NO_2 surface measurements at 13:00-14:00 and 10:00-11:00
LT, updated EPA anthropogenic NO_x emissions, and satellite NO_2 TVCD data over the AQS
urban sites (left column) and the CONUS urban regions (right column) for 4 seasons. AQS NO_2
surface measurements are not included in the right column. All datasets are scaled by their
corresponding values in 2011 except for GOME-2B. For GOME-2B, we firstly normalized the
values in each season to the corresponding 2013 values and plotted the relative changes from the
2013 EPA point of each season to make the GOME-2B relative variations comparable to the
other datasets. Shading in a lighter color is added to show the standard deviation of the results;
when uncertainty is small due in part to a large number of data points, shading area may not show
up.
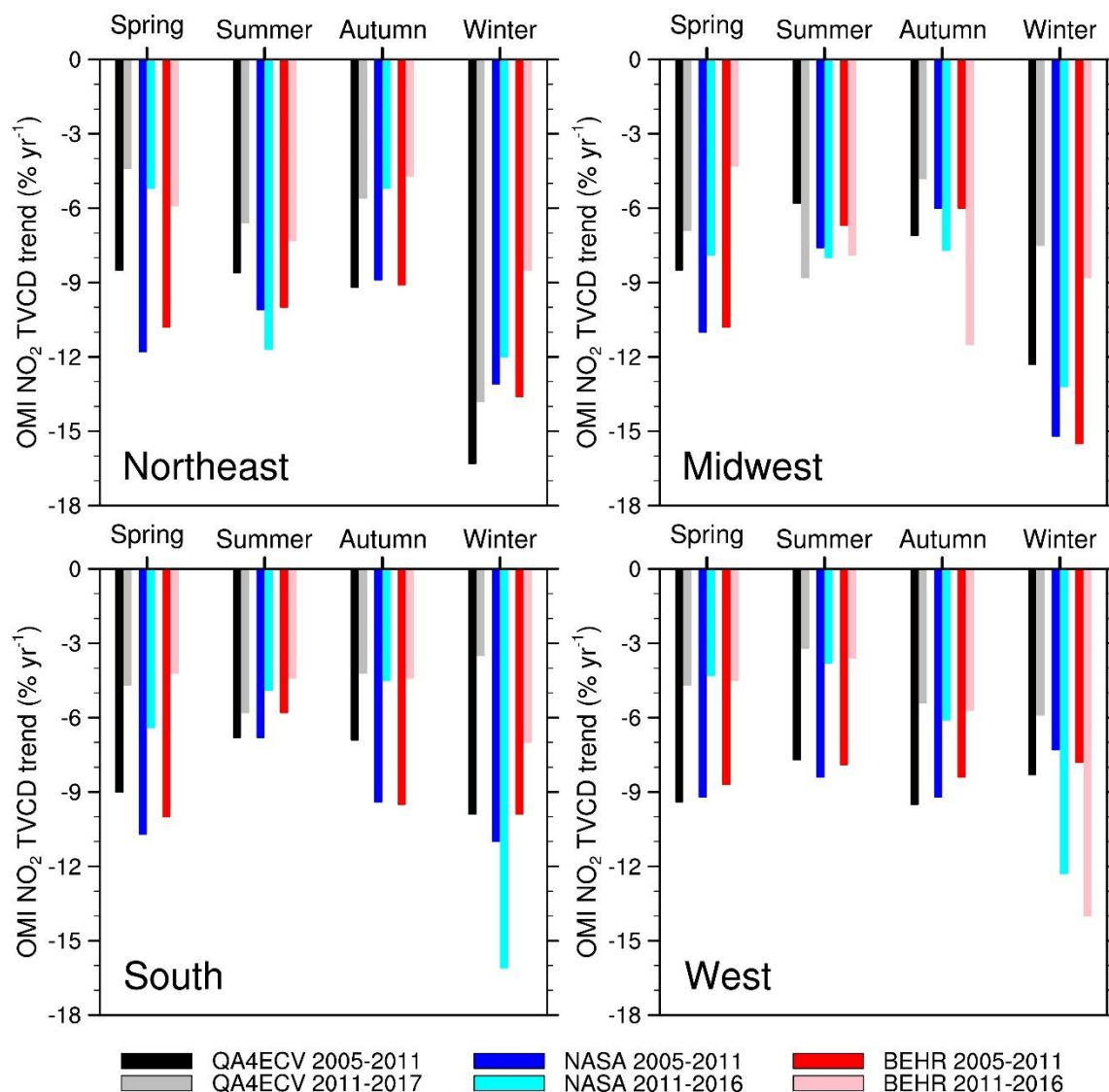
Figure 7. Pre- and post-2011 OMI NO_2 TVCD trends for 4 seasons in the urban regions of Northeast, Midwest, South, and West. Black bars denote OMI-QA4ECV NO_2 TVCD trends from 2005 – 2011; gray bars denote the corresponding trends during 2011 – 2017. Blue bars denote OMI-NASA trends from 2005 – 2011; cyan bars denote NASA-OMI trends from 2011 – 2016. Red bars denote BEHR-OMI trends from 2005 – 2011; pink bars denote OMI-BEHR trends from 2011 – 2016.